Nanorheology and boundary slip in confined liquids using atomic force microscopy

2008 J. Phys.: Condens. Matter 20 315201

(http://iopscience.iop.org/0953-8984/20/31/315201)

IOP Publishing Journal of Physics: Condensed Matter

J. Phys.: Condens. Matter **20** (2008) 315201 (11pp) doi:10.1088/0953-8984/20/31/315201

Nanorheology and boundary slip in confined liquids using atomic force microscopy

Abdelhamid Maali[1] **and Bharat Bhushan**[2,3]

[1] Centre de Physique Moléculaire Optique et Hertzienne, Université Bordeaux 1, 351 cours de la Libération, F-33405 Talence, France

[2] Nanoprobe Laboratory for Bio- and Nanotechnology and Biomimetics, Ohio State University, 201 W. 19th Avenue, Columbus, OH 43210-1142, USA

E-mail: bhushan.2@osu.edu

Received 18 April 2008, in final form 2 June 2008
Published 17 July 2008
Online at stacks.iop.org/JPhysCM/20/315201

Abstract

The physical properties of materials at the nanometer scale can be completely different from those of the bulk. Here we review some of the properties of confined liquids using an atomic force microscope (AFM). We present different experimental schemes used to study layering of the liquid confined between an AFM tip and solid substrate. Then we consider the liquid flow close to the solid wall and report some experimental measurements of the liquid slip on different surfaces using colloidal particles glued to an AFM cantilever. Nanobubble formation on hydrophobic surfaces is also described at the end of the paper.

(Some figures in this article are in colour only in the electronic version)

1. Introduction

The atomic force microscope (AFM) provides a sensitive force sensor [1–9]. Therefore AFMs are widely used to investigate the mechanical properties and structure of materials at the nanometer scale. The surface topography and various properties of organic and inorganic surfaces have been obtained with high resolution in vacuum [4], in air and in liquid [3, 5].

Image contrast arises because the interaction force between the cantilever tip and sample depends on the tip-to-sample distance and also on the properties of the sample. Alternatively, one can measure, at a given position on the sample, the interaction between the tip and the sample versus the separation. These measurements are known as force measurements [7–9]. In the contact mode, the cantilever tip is moved toward the substrate in the normal direction, and the deflection of the cantilever is recorded and converted to force versus tip–substrate separation [7, 8]. In the dynamic mode [9], the tip is vibrated during the approach to the substrate, and both the amplitude and phase is recorded in amplitude modulation mode (AM-AFM), and the frequency shift and the damping are recorded in the frequency modulation mode (FM-AFM).

The AFM measures not only the interaction between the tip and the substrate but also the properties of the medium between them. When the medium is a fluid, the rheological properties can be investigated at scales varying from nanometers up to a few micrometers by varying the cantilever to substrate separation [8].

The physical properties of materials at the nanometer scale can be completely different from those of the bulk. In particular, striking phenomena occur at the nanometer scale where the molecular structure of the liquid and the properties of liquid–solid interaction become predominant. As an illustration, the rheological properties of a fluid confined between two surfaces depend crucially on the ratio of the molecular size σ and the thickness of the fluid layer d. Liquid confined between two surfaces can form ordered layers which lead to an oscillatory solvation force that acts on the surfaces. Confined liquids have been extensively studied using a surface force apparatus (SFA) [10–23] and atomic force microscopy (AFM), which will be described in detail in section 2.

The properties of the fluid near the surfaces also play a major role in hydrodynamics [24]. Indeed, an important

[3] Author to whom any correspondence should be addressed.

assumption in hydrodynamics is the so-called non-slip boundary condition for the flow of a liquid near a solid surface: the fluid molecules are assumed to stick to the solid surface and the fluid velocity is set equal to the respective velocity of the surface. This assumption, however, is not always valid as recent experimental developments have shown [24]. Now, it is possible to manipulate and control systems at the micrometer and nanometer scales, thanks to recent developments in SFA and AFM. Several experiments recently carried out [24, 25] demonstrate an apparent slip of Newtonian liquids near solid surfaces, suggesting that the apparent slip is not an artifact. Attempts to explain the wide range of measured slip lengths are underway. Using the AFM, some experiments show that the slip length depends on the shear rate and also on the roughness of the surface [25]. To explain the origin of the slip, the presence of gas bubbles on the solid surface [26, 27] was invoked, on which the liquid molecules can move freely. Nanobubbles are found to appear spontaneously at the interface between a polar solvent (e.g. water) and a hydrophobic surface. These have been the subject of extensive research using AFM [28].

In this paper, we present a review of the nanorheology of confined liquids and boundary slip of liquids close to solid surfaces. Nanobubble formation on hydrophobic surfaces is also discussed.

2. Nanorheology of confined liquids

Ordering of liquids at interfaces is a phenomenon of fundamental importance and has been of interest in several fields of research such as tribology [10, 11], nanofluidics [12] and biology [13]. Liquid ordering as induced by confinement between two solid surfaces leads to an oscillatory force that acts on the surfaces. This force arises from the variation of liquid properties (molecular density) between the surfaces. For geometrical reasons, the confined liquid molecules may pack to result in higher density which depends on the gap between the confining surfaces. The experiments show that the oscillatory solvation force (force acting on surfaces confining a fluid) has a period of oscillation approximately equal to the molecular diameter. The amplitude of this oscillatory force decreases as the gap between the surfaces is increased. Liquid ordering and solvation force have been extensively studied using SFA [12–21]. In this section, we review some of the work done using an atomic force microscope both in contact mode [29–32], where the tip is not vibrated, and in dynamic mode [33–46], where the tip is vibrated.

2.1. Contact mode

In contact mode, the liquid layering is measured by monitoring the DC deflection of the cantilever [29]. As the thickness of the liquid film confined between the tip and the surface is reduced, the amplitude of the solvation force acting on the cantilever increases (equation (A.2) in the appendix). For a calibrated cantilever, the measurements of the deflection directly provide the force versus the tip–surface distance by multiplying the deflection with the spring constant of the cantilever. For such an experiment, a soft cantilever is chosen in order to resolve the induced deflection from the noise. Franz *et al* [30] showed that short linear alcohols ($C_nH_{2n+2}O$, $n = 2$–8) organize differently on mica and graphite surfaces. On the hydrophilic surface, the oscillatory profile had a period longer than the length of a single molecule and increased proportionally to the chain length, suggesting that the molecules are in an upright position, forming a double layer. On the hydrophobic substrate, the oscillation of the force profile was independent of the chain length, indicating that the molecules lay flat on the surface [30]. Solvation force was also measured in this mode for ionic liquids at room temperature [31]. The liquids studied were ethylammonium nitrate (EAN), propylammonium nitrate (PAN) and 1-ethyl-3-methylimidazolium acetate (C_2mimAC). The measurements reveal an oscillatory behavior with a period corresponding to the dimension of the ion pair (figure 1). The surface charge and roughness and the orientations of cations at the interface are critical determinants of solvation layer formation in ionic liquids. The greatest number of solvation periods was obtained with EAN on highly charged atomically smooth mica. Recently, simultaneous force and electrical conductivity measurements have been done on hexadecane confined between an atomic force microscope tip and a graphite surface. Both the current and the force data reveal discrete solvation layering of the hexadecane near the surface [32].

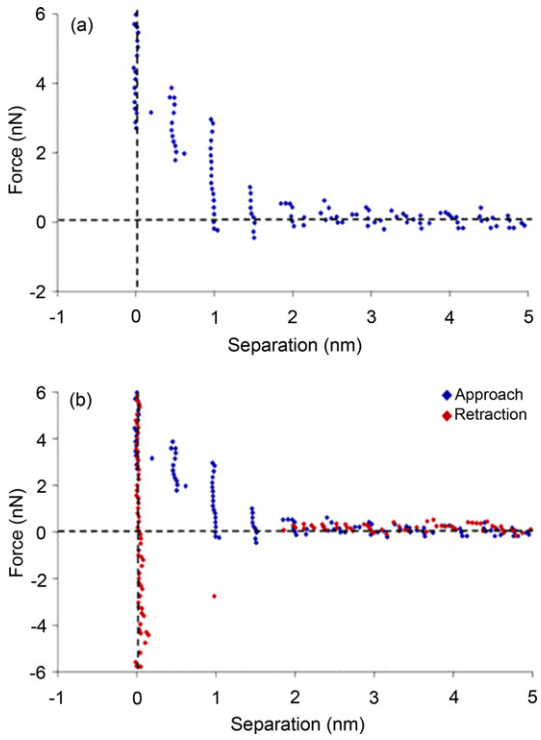

Figure 1. (a) Force versus separation curve for an AFM tip (A) approaching and (b) retracting from the ionic liquid ethylammonium nitrate (EAN) on a mica surface. At least six steps in the force curve can be seen, extending to a separation of 3 nm [31].

2.2. Tapping mode

In tapping mode, the cantilever tip is vibrated at a fixed frequency, and the amplitude and phase of the tip are monitored during the interaction. The tip is approached toward the sample continuously with a small velocity of the order of a few nm per second. To induce vibration of the tip, either the tip is excited by a piezo-actuator or by applying a varying magnetic field on a magnetic coated cantilever. The amplitude and phase variations are measured using a lock-in amplifier.

2.2.1. Calculation of the interaction stiffness and damping in the dynamic mode. The force induced by the confined fluid on the cantilever tip has two contributions; one is a conservative term ($-k_{\text{int}}z$) and the other is a dissipative term ($-\gamma_{\text{int}}\dot{z}$), where k_{int} and γ_{int} are the effective interaction stiffness and damping coefficient of the confined liquid, and z is the instantaneous position of the cantilever. The motion of the cantilever is then described by

$$m^*\ddot{z} + (\gamma_0 + \gamma_{\text{int}})\,\dot{z} + (k_\ell + k_{\text{int}})\,z = F_0 \exp(\mathrm{j}\omega t) \qquad (1)$$

where the driving force, $F_0 = \frac{k_l A_0}{Q}$, m^* is the effective mass of the cantilever, and γ_0 is the viscous hydrodynamic damping far from the surface and is related to the quality factor Q and the resonance frequency ω_0 via the equation $Q = \frac{m^*\omega_0}{\gamma_0}$; k_ℓ is the cantilever stiffness and A_0 is the amplitude of the oscillation far away from the interaction region. The solution $z = A\exp\mathrm{j}(\omega t + \varphi)$ of equation (1) gives the stiffness and the damping coefficient:

$$k_{\text{int}} = k_\ell\left(\frac{A_0\cos(\varphi)}{AQ} - 1 + \frac{\omega^2}{\omega_0^2}\right) \qquad (2)$$

and

$$1 + \gamma_{\text{int}}/\gamma_0 = -\frac{\omega_0 A_0}{\omega A}\sin(\varphi) \qquad (3)$$

where A and φ are, respectively, the measured amplitude and phase of the oscillation, and ω is the driving frequency of the cantilever. ω_0 and A_0 are the resonance frequency and the amplitude of the cantilever without interaction.

When working far below the resonance frequency of the cantilever ($\omega \ll \omega_0$), the amplitude of the tip vibration at this frequency far from the interaction region is $A_0(\omega) \approx \frac{A_0(\omega_0)}{Q}$ and $\cos(\varphi) \approx 1$. Then equation (2) becomes

$$k_{\text{int}} = k_l\left(\frac{A_0(\omega)}{A} - 1\right). \qquad (4)$$

2.2.2. Off-resonance tapping-mode experiments. The first AFM experiment on liquid ordering was carried out by O'Shea *et al* [33]. They used a magnetic tip that vibrated off-resonance, and they showed evidence of up to seven ordered layers of liquid at an interface with graphite. However, the spacing between layers of the quasi-spherical molecule studied, OMCTS, was substantially smaller (0.5 nm) than the smallest known dimension of the molecule (0.8 nm). Han and Lindsay [34] repeated these measurements with a PicoSPM from Molecular Imaging (Phoenix, AZ) operated in the magnetic a/c mode (MAC Mode). Figure 2 shows two typical force spectra at OMCTS–graphite interfaces. They demonstrate the reproducibility of the spectra obtained with different tips. In both figures, seven layers of OMCTS molecules at the interface are clearly detected. The average spacing between two adjacent layers during trace and retrace was about 0.82 nm, consistent with molecular dimensions.

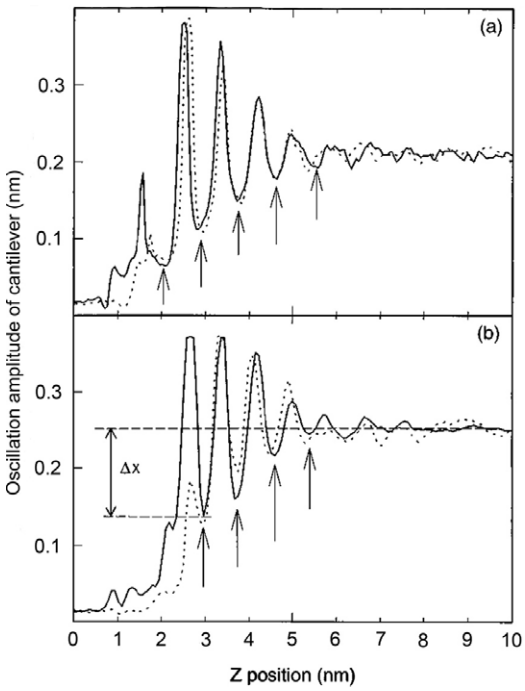

Figure 2. Two independent measurements of force spectra of the MAC Mode AFM at OMCTS–graphite interface. The amplitude of oscillation of the magnetic cantilever driven by an external magnetic field oscillates in both approaching (solid line) and retracting (dotted line) curves in the region of a few nanometers away from the surface due to ordered layers of OMCTS molecules at the interface. The period of the oscillation, 0.82 nm, precisely reflected the dimension of OMCTS molecules along the direction perpendicular to the layers, (a) driving frequency 500 Hz, scan rate 2.8 nm s^{-1}, and (b) driving frequency 200 Hz, scan rate 1.6 nm s^{-1}. The arrows correspond to repulsive-force maxima [34].

To study the confined OMCTS on a graphite surface, Lim *et al* [35] used off-resonance, sample modulation atomic force microscopy, where the sample is modulated at low amplitude and far from the cantilever resonance frequency. The interaction stiffness due to liquid ordering was measured as a function of the tip–sample distance. Figure 3 shows representative force curves for OMCTS on graphite. Figure 3(a) shows the normalized amplitude and applied force plotted against the tip–sample distance (D). The dotted lines show that the amplitude maxima correspond to alternating applied force maxima and minima. Figure 3(b) is a plot of stiffness as calculated from the normalized amplitude data. The peak-to-peak stiffness values are measured from the stiffness minimum to stiffness maximum as indicated by the arrows and vary from 3 to 1.5 to 0.7 to 0.3 N m^{-1} for the first, second, third and fourth solvation layers, respectively. As the gap is increased the stiffness decreases as predicted by equation (A.3) in the appendix. Upon integration of the stiffness with respect

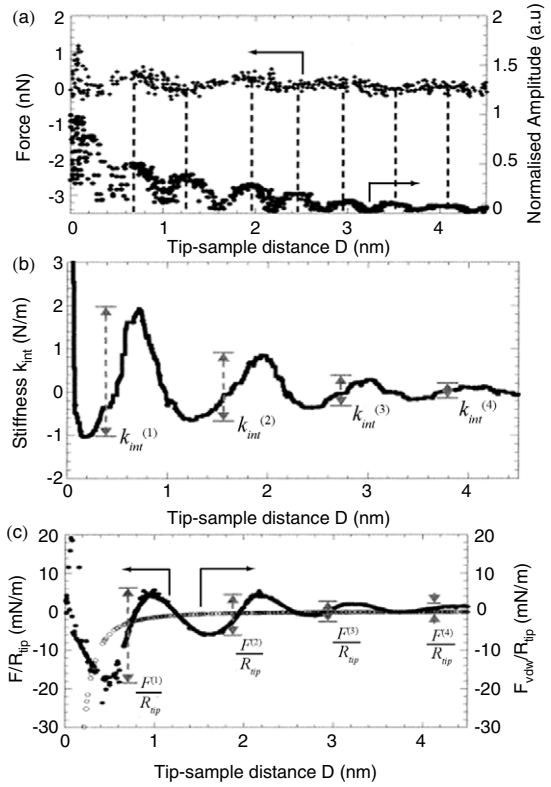

Figure 3. Force versus distance curve from a single approach measured in OMCTS ($k_c = 2.5$ N m^{-1}, $\omega/\omega_0 = 0.006$, $R_{tip} = 26$ nm). (a) Applied force and normalized amplitude plotted as a function of separation. The dotted lines indicate that each amplitude maximum corresponds (alternatively) to either an applied force maximum or an applied force minimum. (b) Amplitude data, converted into stiffness (k_{int}), as a function of separation. The peak-to-peak stiffness values for the first, second, third and fourth solvation layers ($k_{int}^{(1)} - k_{int}^{(4)}$) are measured to be 3, 1.5, 0.7 and 0.3 N m^{-1}, respectively. (c) Normalized force (F/R_{tip}) as a function of separation, as calculated by integration of the stiffness data of figure 3(b). F/R_{tip} values for the first, second, third and fourth solvation layers ($F^{(1)}/R_{tip}$–$F^{(4)}/R_{tip}$) are measured to be 24, 13, 5 and 2.5 mN m^{-1}, respectively. Also shown is the estimated van der Waals force for the SiO_2–OMCTS–HOPG system [35].

to the tip–sample distance, the force can be calculated and normalized by the tip radius (figure 3(c)). Normalization allows for a comparison between this present work and similar AFM or SFA data. The normalized forces corresponding to the first, second, third and fourth solvation layers are measured to be 24, 13, 5 and 2.5 mN m^{-1}, respectively.

Jeffery *et al* [38] have studied an aqueous solution of 10 mM KCl confined between mica and a silicon tip using a modified atomic force microscope. The tip was vibrated at a very low amplitude, 0.036 nm, and at a frequency far below the cantilever resonance frequency. From the measured amplitude and variation signals, they show the presence of up to seven molecular layers having a thickness of 0.25 nm.

Layering of confined water was also measured by a shear force microscope [39, 40]. In such experiments, a sinusoidal shear strain was applied by vibrating the tip laterally (in the direction parallel to the sample). The measurement of the lateral amplitude of the tip and the phase at different tip–

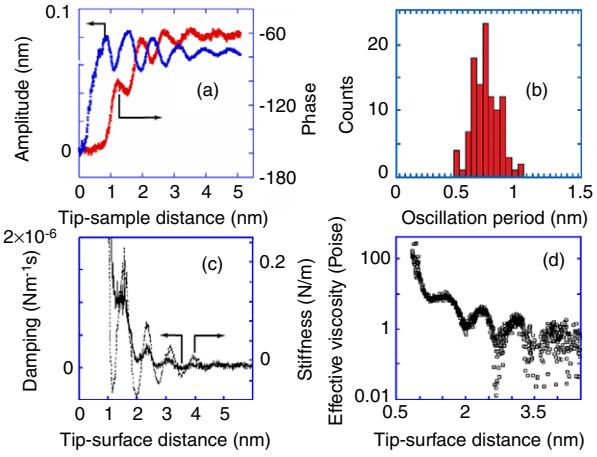

Figure 4. (a) Amplitude and phase of the cantilever as the tip approaches the surface, (b) histogram of the measured oscillation period in the amplitude signal, (c) the interaction stiffness (dotted line) and damping (continuous) of the confined liquid versus the gap between the cantilever tip and the substrate, and (d) effective viscosity as the tip approaches the surfaces extracted from the data of the damping [41].

sample separations exhibits a step-like behavior [39]. The periodicity recorded over several curves ranged between 0.24 and 0.29 nm, which is similar to the diameter of the water molecule.

2.2.3. Close to resonance tapping-mode experiments. In order to increase the sensitivity, it is useful to work close to resonance. Maali *et al* [41] have used tapping-mode AFM to study the ordering of OMCTS on graphite surfaces. They used a MikroMasch cantilever with a resonance frequency in liquid of 32.2 kHz and a quality factor Q of 3.7. The nominal tip radius was 10 nm, and the spring constant was $k_l = 0.95$ N m^{-1}. The cantilever was vibrated at amplitudes ranging from 0.08 to 0.32 nm using a modified excitation cantilever holder [42]. The data are obtained by varying the tip–sample separation and recording the vibration amplitude and phase of the cantilever. Figure 4(a) presents the amplitude and phase recorded as the tip approaches the surface. Several oscillations in the curves can be clearly observed. The average periodicity measured over 20 approach–retract cycles is 0.78 nm, figure 4(b).

From the amplitude and phase data, they calculated the interaction stiffness and the damping coefficient for the cantilever amplitude of 0.08 nm. Figure 4(c) presents the interaction stiffness and damping versus tip–substrate distance. Similarly to the amplitude and phase curves, the modulation of the stiffness with a periodicity equal to the molecular diameter is observed. The maxima of the interaction stiffness correspond to situations in which the liquid is denser than the bulk and the cantilever senses a force pushing the tip as it enters the layer. The zero values correspond to situations in which the liquid density is similar to that of the bulk. The minima of the stiffness correspond to situations in which the fluid density below the tip is smaller than the bulk density and thus inducing a force over the tip motion. The explanation of the variation

of the stiffness by a variation of the density is supported by Heuberger *et al* [23], in which density fluctuations induced by confinement have been reported using an improved SFA apparatus. For distances greater than 5 nm, the interaction damping is zero. As the tip approaches the surface, the damping shows two features: a periodic variation and an increase. The damping modulation period is equal to the molecular diameter. Notice that the damping is in phase with the stiffness curve. When the tip–surface distance is equal to a multiple of the molecular diameter (distances corresponding to the maxima of the stiffness), the damping is higher, and for distances corresponding to a multiple and a half of the diameter, the damping is at a minimum.

One can compare the measured damping to the hydrodynamic damping. At 1 nm from the surface and with a tip radius $R = 10$ nm, $\gamma_{\text{hydro}} = 4.2 \times 10^{-9}$ N m^{-1} s, $\gamma_{\text{int}} = 2 \times 10^{-6}$ N m^{-1} s. Assuming a constant value of the viscosity ($\eta = 0.022$ P) leads to very small dissipation ($\gamma_{\text{Hydro}}/\gamma_{\text{int}} = 0.002$). The increase of the damping cannot be described by a hydrodynamic force acting on the cantilever tip moving in a fluid behaving like a bulk fluid with a constant viscosity. Klein and Granick and others [18–20] reported an increase of viscosity of confined OMCTS. Their measurements are based on shearing the SFA confining surface laterally and measuring the frictional force. In the SFA experiment during the approach, the surface separations D for a film of thickness $n\sigma$ are measured only from $n\sigma$ to $(n + 1/2)\sigma$. The distance range $(n + 1/2)\sigma < D < (n + 1)\sigma$ is not accessible because of the finite spring constant of the apparatus. Also, due to a limited number of measurements versus the surface gap in those experiments, they reported only an increase of viscosity. In the AFM experiment Maali *et al* [41] had access to a nearly continuous tip–surface gap variation. The gap is varied in steps of 4 pm. For each cantilever tip–surface distance, the confined liquid can be described by a fluid having an effective viscosity, $\eta_{\text{eff}}(D)$:

$$\eta_{\text{eff}} = \frac{\gamma_{\text{int}} D}{6\pi R^2}. \tag{5}$$

The effective viscosity is extracted from the damping data and is shown in figure 4(d). The viscosity is not only increasing as reported earlier in SFA experiments but is also modulated. The viscosity modulation length is equal to the molecular diameter. The uncertainty of the measurements is of the order of 0.1 P, which is sufficient to show the modulation of the viscosity. For films of thickness corresponding to one monolayer the viscosity is larger than 200 P, which is four orders of magnitude larger than the bulk viscosity. Notice here that, in contrast to SFA experiments where one measures shear stress and derives the viscosity by assuming the couette flow geometry, the viscosity is measured in this experiment by a normal approach of the tip to the surface.

2.3. Frequency modulation experiments

Various researchers [43–46] have used the frequency modulation atomic force microscope (FM-AFM) to study confined liquids. In this mode, the monitored values are the frequency shift and the excitation voltage that is supplied to the cantilever in order to maintain the vibration amplitude as constant. They have studied several liquids on different surfaces (OMCTS on graphite surface, and water on mica and phospholipid-coated surfaces). Water confined between a carbon nanotube attached to a cantilever and a self-assembled monolayer of alkane thiols undergoes layer ordering that induces an oscillatory profile in the frequency shift [45]. A close inspection of the size variation of the molecular layers of the proximity to the surface reveals the layer thickness increases slightly with the distance from the surface.

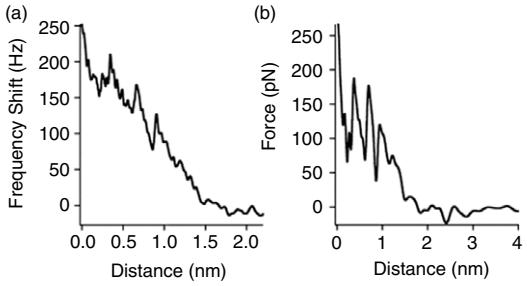

Figure 5. (a) Frequency shift versus distance curves for the gel phase bilayer (24 °C) reveal three oscillations superimposed on a background repulsive interaction, (b) conversion of the frequency shift curve to a quantitative force clearly revealed the oscillatory nature of the hydration force that spanned a few hundred piconewtons, with each oscillation recording a range of ≈100 pN [46].

Also using FM-AFM, the hydration force between the probe and lipid bilayer surface that mimics a biological membrane surface was observed [46]. The force was extracted from the frequency shift during a vertical approach of the tip to the surface using a mathematical model [44]. The force has an oscillatory profile that reflects the removal of up to five structured water layers from the membrane (figure 5). Further, they found that the hydration force can be modified by changing the membrane fluidity.

In comparison to tapping mode, the frequency modulation mode offers the advantage that the elastic part (frequency shift) and inelastic part (damping) can be measured directly during the tip interaction with the confined liquid.

3. Boundary slip

The non-slip boundary condition at a solid interface is at the center of our understanding of fluid mechanics. The fluid velocity is assumed to be equal to the respective velocity of the surface. Recent experimental developments, allowing one to manipulate and control systems at the micrometer and nanometer scales, have opened the way to severe tests of the non-slip boundary condition. Several experiments demonstrate an apparent slip of Newtonian liquids near solid surfaces [47–63]. The variety of methods used indicates that the observed slip is not an artifact of a single technique, but opens the debate to explain the wide range of the measured slip lengths.

The situation for a simple shear flow is schematically presented in figure 6. The upper surface is moving with

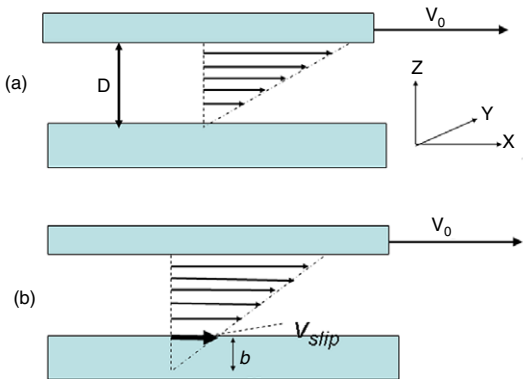

Figure 6. Schematic representation of velocity profile of the liquid versus the gap between two surfaces. The upper surface is moving with velocity V_0 and the lower surface is at rest for (a) the non-slip boundary conditions on both surfaces and (b) the slip condition at the lower surface. In (b) slip occurs at the lower surface by an amount v_{slip}. The extent of slip is characterized by the slip length (b).

velocity v_0 and the lower surface is at rest. In the case of non-slip boundary conditions, the molecules' velocities are equal to the walls' velocities (figure 6(a)). In the slip conditions on the lower surface, the molecules' velocities on the lower surfaces are different from the wall velocity and equal to $v_{\text{slip}} = b\frac{\partial v}{\partial z}$ where b is the fictitious distance below the surface where the non-slip boundary conditions would be satisfied (figure 6(b)).

3.1. Basic hydrodynamic theory for a sphere–plane wall geometry

Navier–Stokes equations describe most of the phenomena occurring during the fluid flow. The first equation is derived from the incompressibility criterion together with the mass conservation [64, 65]:

$$\nabla\vec{v} = 0 \tag{6}$$

where $\vec{v}$ is the velocity of the fluid. The second equation is derived by applying Newton's second law of motion to a small block of fluid:

$$\rho\frac{\partial\vec{v}}{\partial t} = -\vec{\nabla}p + \eta\Delta\vec{v} - \rho\vec{v}\nabla\vec{v} \tag{7}$$

where ρ is the fluid density, η is the viscosity and p is the pressure. In this later equation the gravitational force is neglected. Solving these equations allows one to determine the pressure and the velocity profile of a fluid. The solutions depend on the geometry of the system and on the boundary conditions on the interfaces.

For a sphere approaching a flat surface, the solution was calculated analytically, especially in the lubrication approximation, where the distance between the sphere and the solid flat surfaces is very small compared to the sphere radius (see figure 7). For the case of non-slip boundary conditions which require that the molecules directly in contact with the surfaces stick to the surfaces and do not slip laterally $\frac{\partial v\ell}{\partial z} = 0$ (v_ℓ is the lateral velocity of the fluid molecules). For this case the expression of the hydrodynamic force acting on the

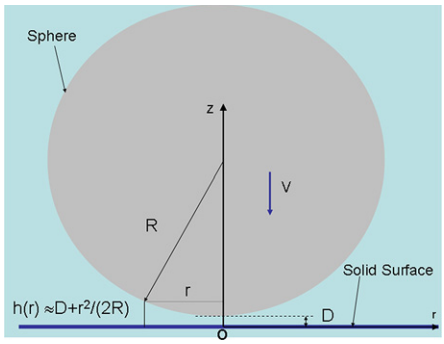

Figure 7. A sphere of radius R immersed in a liquid approaches a solid surface with a velocity V. When $D \ll R$, the distance between the sphere and the solid surface is given by $h(r) \sim D + \frac{r^2}{2R}$.

sphere is[4]

$$F = \frac{6\pi\eta R^2}{D}\frac{\mathrm{d}D}{\mathrm{d}t} \tag{8}$$

where $\frac{\mathrm{d}D}{\mathrm{d}t}$ is the velocity of perpendicular approach of the sphere to the plane surface and D is the gap between the two surfaces. This expression is known as the Taylor equation.

Beyond the lubrication approximation at an arbitrary distance, the solution of the Navier–Stokes equation was calculated analytically by Brenner [67]. As in the previous derivation of the Taylor expression, Brenner assumes non-slip boundary conditions on the surfaces. The hydrodynamic force acting on a sphere of radius R approaching a wall with a velocity v is given by

$$F = 6\pi\eta Rv\lambda \tag{9}$$

where

$$\lambda = \frac{4}{3}\sinh\alpha\sum_{n=1}^{\infty}\frac{n(n+1)}{(2n-1)(2n+3)} \times\left[\frac{2\sinh(2n+1)\alpha + (2n+1)\sinh 2\alpha}{4\sinh^2(n+\frac{1}{2})\alpha - (2n+1)^2\sinh^2\alpha} - 1\right]$$

$$\alpha = \cosh^{-1}\left(1+\frac{D}{R}\right).$$

As the distance D becomes small compared to the sphere radius R, $\lambda \approx \frac{R}{D}$ and the Brenner equation is reduced to Taylor's equation. For very large distances (D tending to infinity), the Brenner equation is simply reduced to the Stokes equation $F = 6\pi\eta Rv$ (force acting on a sphere moving in a bulk fluid).

3.2. Boundary slip conditions

In this section, we present the solution for the Navier–Stokes equation of a sphere approaching a wall in the case of the presence of partial slip boundary conditions on the surfaces. Using these boundary conditions, Vinogradova [68] calculated

[4] This equation is attributed in most texts to G I Taylor (1925), even though it seems that he never published the result of his calculation. The discussion of the origin of the equation was discussed in note 38 of the paper of Horn *et al* [66].

the force acting on the sphere when it approaches the wall. The calculation was made in the lubrication approximation as for Taylor's solution. The solution has the form of Taylor's expression corrected by a factor f:

$$F_h = \frac{6\pi\eta R^2}{D}\frac{\mathrm{d}D}{\mathrm{d}t} f^*(D). \tag{10}$$

The correction factor f^* characterizes the slip boundary conditions. For the symmetric case where the slip occurs on both surfaces (sphere and flat wall), assuming the same amount of slip length b, the correction function is

$$f(D) = \frac{D}{3b}\left[\left(1+\frac{D}{6b}\right)\ln\left(1+\frac{6b}{D}\right)-1\right]. \tag{11}$$

This correction is usually used to describe the drainage of liquid between two hydrophobic surfaces.

For the asymmetric case, the slip occurs only on one surface that is assumed to be hydrophobic and the other surface is hydrophilic. Then the correction is

$$f^* = \frac{1}{4}\left\{1+\frac{6D}{4b}\left[\left(1+\frac{D}{4b}\right)\ln\left(1+\frac{4b}{D}\right)-1\right]\right\}. \tag{12}$$

Note here that the Vinogradova correction f^* assumes a constant slip length b that does not depend on the distance and shear rate.

3.3. Contact mode

The pioneering experiment on liquid slip over surfaces was done in contact mode. A spherical particle with a size ranging from 10 to a few tens of μm is glued to an AFM cantilever. In these experiments, the cantilever was not vibrated during the approach of the lower surfaces to the sphere. The measured value is the cantilever deflection induced by the hydrodynamic force applied on the sphere versus the piezo displacement. From this, the force is calculated by multiplying the cantilever deflection with the spring constant of the cantilever. The particle–surface distance is obtained by subtracting the cantilever deflection from the piezo displacement. The velocity of the approach is set in these experiments to a very high value (ranging from a few μm s^{-1} to a few tens of μm s^{-1}) [57–60].

This technique was used to study a wide range of substrates and liquids. Shear-rate-dependent slip was observed on partially [57] and completely wetting surfaces [58]. Figure 8 shows the measured hydrodynamic drainage force (drag force) of an aqueous medium between smooth hydrophilic surfaces up to a shear rate of typically 10^4 s^{-1} [58]. A silica sphere (radius of $\sim$10 μm) was pushed towards a flat silica surface with different velocities of 4 and 40 μm s^{-1}. The measured force curves were compared to simulations. To reach agreement between experimental and simulated force curves, the hydrodynamic force had to be fitted with a model allowing for boundary slippage characterized by a slip length of 8–9 nm.

Simultaneous observations of molecular layered structure of the liquid and hydrodynamic slip were shown by Sun *et al* [59]. The effect of surface roughness was also studied, and it

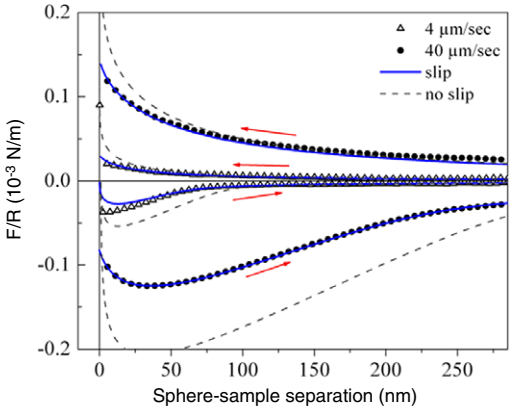

Figure 8. The measured hydrodynamic drainage force of an aqueous medium (200 mM NaCl, pH = 5) between smooth hydrophilic surfaces up to a shear rate of typically 10^4 s^{-1}. A silica sphere (radius $\sim$10 μm) was pushed towards a flat silica surface with different velocities of 4 and 40 μm s^{-1}. The measured force curves were compared to simulations. To reach agreement between experimental and simulated force curves, the hydrodynamic force had to be fitted with a model allowing for boundary slippage characterized by a slip length of 8–9 nm [58].

was demonstrated that the degree of slip increases (from 10 to 175 nm) as the surface roughness increases (from 2 to 50 nm peak to peak) [60]. Recently, a non-slip boundary condition was reported for a hydrophilic glass particle during a rapid approach (1–100 μm s^{-1}) to a hydrophilic glass plate in a viscous sucrose solution [69]. The authors of the later experiment used a stiffer cantilever and used an evanescent optical wave to measure the separation accurately, which may explain the discrepancy with the earliest experiments described above [58, 60].

3.4. Dynamic mode

Recently, dynamic AFM has been used to study liquid flow close to a solid surface [61, 62]. The dynamic mode experiment differs from previous AFM measurements of the slip length which are carried out in the static mode, i.e. the monitored value is the deflection induced by the hydrodynamic force opposing the tip as it approaches the lower surface at high velocity. In such experiments, the distance between the surfaces is given by the imposed displacement plus the tip deflection due to the viscous hydrodynamic force. In the experiments by Maali *et al* [61] and Lasne *et al* [62], the tip is vibrated at a very low amplitude (a few nm), and the amplitude and phase are measured as the tip approaches the surface at a very low velocity, giving the dissipation coefficient with high accuracy. The average hydrodynamic force is zero in these experiments, and the distance between the tip and the surface is given directly by the imposed displacement.

The measurements done in dynamic mode were performed close to resonance. In the Lasne *et al* [62] experiment, a glass sphere of 14 μm diameter was glued on the tip side of the gold-coated silicon nitride cantilever. A measurement of the amplitude of vibration of the cantilever is sufficient to extract the hydrodynamic damping coefficient [70] as the gap

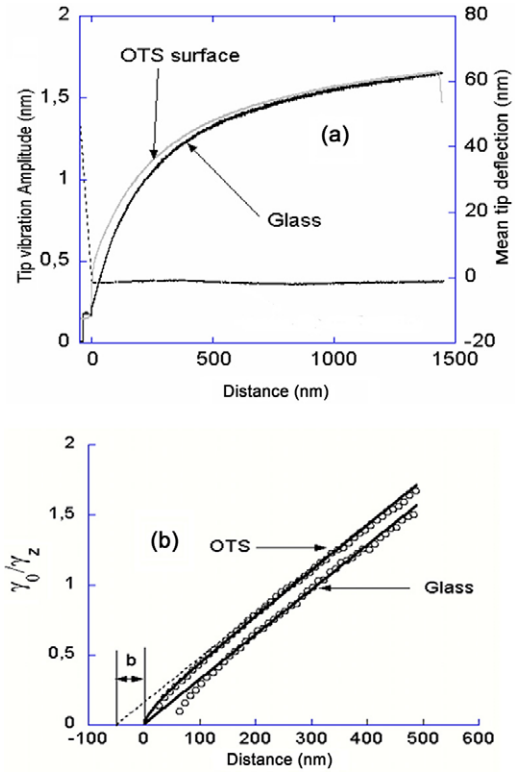

Figure 9. (a) The vibrational amplitude of the sphere as it approaches the glass and OTS surface in water. The line at the bottom represents the DC-deflection signal that allows obtaining the contact position with a resolution of 2 nm. (b) The inverse of the hydrodynamic damping versus the distance extracted from the vibration amplitude data. The solid lines are fits using the no-slip boundary condition (glass slide) and a slip length of 50 nm for the OTS-covered slide. The dashed line extrapolates the data to zero and intercepts the zero axis at a value of b of about 50 nm [62].

between the surface and the sphere diminishes. The surface approaches the sphere with a velocity of 0.2 μm s^{-1} with no noticeable effect on the cantilever mean deflection, as shown in figure 9(a). The surface position was obtained by monitoring the mean deflection of the cantilever, which is zero from the surface, and increases very rapidly at contact as shown in figure 9(a). The resolution on the vertical approach distance is better than 2 nm. For a sphere at a distance z from a solid surface, the hydrodynamic damping coefficient γ_h is given by $\gamma_h = \frac{6\pi\eta R^2}{D} f^*(D)$. Figure 9(b) shows the inverse of the hydrodynamic damping $\frac{\gamma_0}{\gamma_h}$ (γ_0 is the bulk damping) for the two surfaces as extracted from the amplitude–distance curve. The data for glass is fitted assuming no slip on either the sphere or the surface. This figure shows that $\frac{\gamma_0}{\gamma_h}$ is a straight line intercepting the z axis at zero, as expected for the non-slip boundary condition. For the OTS-covered glass slide, however, slip on the bottom surface needs to be taken into account. Indeed, extrapolation of the data to zero as shown by the dashed line intercepts the z axis at a value of about -50 nm. The hydrodynamic dissipation is, in this case, corrected by a factor

$$f^* = \frac{1}{4}\left\{1 + \frac{6D}{4b}\left[\left(1 + \frac{D}{4b}\right)\ln\left(1 + \frac{4b}{D}\right) - 1\right]\right\}.$$

The inverse dissipation on the OTS-covered surface can be fitted to $(\frac{6\pi\eta R^2}{D} f^*)^{-1}$ as shown by the solid line with a value of b (the slip length) of 50 nm $\pm$ 10 nm.

The same technique was used to measure the hydrodynamic damping of an AFM cantilever tip immersed in water and approaching a mica surface or a graphite surface [61]. Water completely wets the mica surface while it partially wets the graphite surface with a contact angle of 74°. The measurements show that the damping is higher on mica than on graphite. By fitting the damping data, a slip length of 8 nm for water flowing on graphite was extracted, while on mica the slip length turns out to be too small to be measured (<2 nm).

Henry *et al* [63] used an alternative dynamic mode method to analyze the hydrodynamic interaction. They used a custom-built nanorheology-atomic force microscope to measure the drainage force between a borosilicate probe and a flat mica surface in pure water and in solutions of a cationic surfactant (cetyltrimethylammonium bromide, CTAB). A low amplitude (5.25 nm) vibration signal of frequency ranging between 600 and 1200 Hz was superimposed to the slow motion of the piezoelectric scanner that approaches the substrate to the sphere. The amplitude and phase change of the cantilever vibration were measured versus the surface separation. From the ratio of the applied amplitude A_0 and the measured cantilever amplitude A, they calculated the effective mobility G versus the separation D [63–71]:

$$G = \frac{12\pi^2\nu R^2}{k\sqrt{(\frac{A_0}{A})^2 - 1}} = \frac{D}{\eta},$$

where ν is the vibration frequency, R is the sphere radius, η is the viscosity and k is the cantilever stiffness. In the plot of the mobility G versus D, the slip length is the position at which the extrapolation of the mobility G intercepts the abscissa line. Their experimental results show that the dependence of the slip on the local shear rate is suppressed if surfactant molecules are adsorbed on the solid surface [63]. Furthermore, when the surfaces are partially covered by surfactant molecules, a similar degree of slippage is measured on hydrophilic and hydrophobic surfaces.

4. Nanobubbles

The interface between liquid and surfaces that form a weak intermolecular interaction with the liquid (hydrophobic surfaces) is subject to intensive research. Nanobubbles of 5–100 nm height and 0.1–1 μm diameter are found to appear spontaneously at the interface between a polar solvent (e.g. water) and a hydrophobic surface. They are invoked as the possible origin of the increase in flow rate of liquids in microchannels [26, 27, 72]. It was also invoked that the presence of nanobubbles can explain the liquid slip at the interface and the long range attraction between hydrophobic surfaces in water.

Most of the experimental work showed that nanobubbles behave as soft isolated objects on the surfaces[5]. Agrawal *et al*

[5] Nanobubbles have been reported as isolated objects with the exception of the work reported by Tyrell and Attard [73].

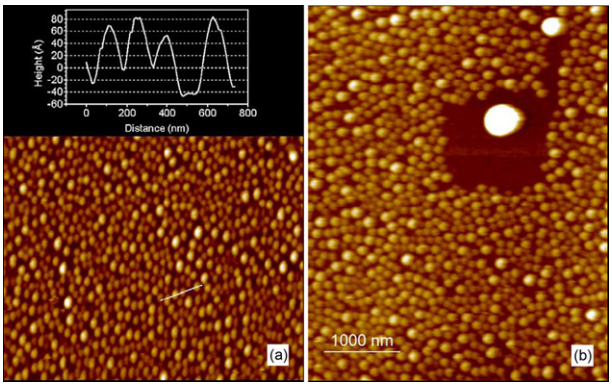

Figure 10. (a) The tapping-mode images obtained on the PS-coated surface when immersed in water. The area coverage of bubbles was measured to be 61 ± 5%. (b) By scanning a small region with increased tapping amplitude, the bubbles in this region are fused into one big bubble (bright object inside the dark square) [78].

[74] reported the control of the location and spatial extent of nanobubbles using hydrophobically nanopatterned surfaces. They found that the degree of surface hydrophobicity and the spatial dimensions of the domains on the nanopatterned surface are the important parameters that control the presence of nanobubbles. The stability of the nanobubbles on the surfaces is another task which has to be studied thoroughly [75–77]. The small bubbles are less stable than the large ones. Simonsen *et al* [78] showed that coalescence can be induced during imaging of the bubbles with a high applied force. Figure 10(a) shows the tapping-mode images obtained on the PS-coated surface when immersed in water. The area coverage of bubbles was measured to be 61 ± 5%. Evidence of the bubbles manipulated by the AFM tip is shown in figure 10(b), where a square area of $1 \times 1\ \mu m^2$ was scanned with increased tapping force. The region was then rescanned with normal tapping force and in an expanded scan window. A big object, different in size from all other objects of the sample, is found in a square region. This proves that the tip movement at increased tapping force can induce a fusion of several small bubbles into one big bubble (bright object inside the dark square).

The coalescence of bubbles can be explained by the Laplace–Young equation: $\Delta p = 2\gamma/R$, where R is the radius of the bubbles, γ is surface tension and Δp is the pressure difference between the inside and the outside of the sphere. For the air/water interface, the surface tension is constant. So, the pressure difference is inversely proportional to bubble radius. Small bubbles have larger inside pressure than bigger ones, and so they are not as stable as bigger bubbles.

Zhang *et al* [79] proposed a new approach to the formation of nanobubbles by manipulating the dissolved gasses. They showed that nanobubbles can be formed even on wetting surfaces like mica. In their experiment, the substrates had been exposed to ethanol.

The different techniques used to prepare bubbles and images open the way to study the viscoelastic properties of the bubbles. AFM in dynamic mode is a powerful tool for this study since it allows measurement of the elastic and inelastic properties of the bubbles. We may expect that the interaction stiffness and damping depend strongly on the shape and size of the bubbles.

On the other hand, the link between the bubbles' presence and the slip length is not yet completely understood. The influence of density and size of the bubbles on the liquid flow needs more investigation.

5. Conclusion

We have reviewed the experimental investigations of the physical properties of a confined liquid. We have shown that, at the nanometer scale, the liquid properties are completely different from those of the bulk.

The first example of this is provided by a liquid confined between two solids in which the liquid undergoes some ordering due to the presence of interactions with the solid wall.

We have described the different techniques used in this study. The contact mode measures the solvation force acting on the tip during approaching the tip to the substrate. The dynamic mode measures the stiffness and the damping of the confined liquid. The dynamic mode offers the advantages of allowing access to both the elastic and inelastic properties of the confined liquid. Thus, it allows one to investigate not only the liquid layering as in contact mode but also to measure the viscosity of the confined liquids.

The second property of liquids at the nanometer scale that we have presented in this paper is liquid slip as it flows on a solid wall. We have presented the contact and dynamic modes used to study a wide range of substrates and liquids. A variety of the values of the measured slip length and also the contradictory results concerning liquid slip on wetting surfaces leave the field open for further investigations. The combination of AFM with an optical microscope in order to measure precisely and independently the tip-to-surface distance reduces the experimental errors.

The last section presents the nanobubble studies. Nanobubbles are found to appear spontaneously at the interface between a liquid and surfaces that form a weak intermolecular interaction with the liquid (hydrophobic surface). Nanobubbles are imaged on different surfaces and behave as soft isolated objects. By increasing the applied force during imaging, the coalescence of the bubbles was demonstrated. The mechanism that promotes bubble nucleation and stabilization of the bubbles on the surfaces is not yet completely understood. The viscoelastic properties of the nanobubbles are another task that will be interesting to investigate.

Appendix. Expression for the interaction stiffness and hydrodynamic damping coefficient

From SFA experiments [17], the solvation force per unit area acting between two flat surfaces has an oscillatory profile which decays exponentially and can be approximated by

$$f(D) \approx p_0 \cos(2\pi D/\sigma) \exp(-D/\tau) \qquad \text{(A.1)}$$

where D is the distance between the two surfaces, σ is the molecular diameter and τ is the decay length of the interaction.

For the AFM contact mode experiment on liquid layering, the measured value is the total solvation force that acts on the tip, and it is calculated by summing $f(D)$ over the surface of the tip. The total force F acting on the cantilever tip for $D < R$ [33]:

$$F(D) = -\frac{p_0 2\pi R\tau\sigma}{\sqrt{\sigma^2 + 4\pi^2\tau^2}} \cos(2\pi D/\sigma + \delta) \exp(-D/\tau) \tag{A.2}$$

with $\tan\delta = \frac{2\pi\tau}{\sigma}$.

The interaction stiffness k_{int} measured in dynamic mode is equal to the gradient of the total force:

$$k_{\text{int}}(D) = -\frac{\partial F}{\partial D} = p_0 2\pi R \cos(2\pi D/\sigma) \exp(-D/\tau) \tag{A.3}$$

where δ is the phase shift. Notice that $F(D)$ and the interaction stiffness k_{int} have an oscillatory profile with an exponential decay that can be measured experimentally. The above expression is oversimplified, but it reproduces the main experimental observations, i.e. the oscillatory variation of the stiffness and the exponential decay profile. Notice that, unlike in SFA experiments, the radius of the AFM tip is not infinite compared to the molecular diameter.

The damping can be calculated using Navier–Stokes equations that give the Taylor force acting on the cantilever tip, as first order [66],

$$F = \frac{6\pi\eta_{\text{eff}} R^2}{D} \frac{\mathrm{d}D}{\mathrm{d}t} \tag{A.4}$$

where R is the tip radius and η_{eff} is the effective viscosity of the confined liquid. D is the gap between the tip and the surface. The hydrodynamic damping coefficient is given as

$$\gamma_{\text{hydro}} = F/(\mathrm{d}D/\mathrm{d}t) = \frac{6\pi\eta_{\text{eff}} R^2}{D}. \tag{A.5}$$

References

[1] Binnig G, Quate C F and Gerber Ch 1986 *Phys. Rev. Lett.* **56** 930
[2] Martin Y, Williams C C and Wickramasinghe H K 1987 *J. Appl. Phys.* **61** 4723
[3] Ohnesorge F and Binnig G 1993 *Science* **260** 1451
[4] Giessibl J F 1995 *Science* **267** 68
[5] Schabert F A, Henn C and Engel A 1995 *Science* **268** 92
[6] Bhushan B 2007 *Springer Handbook of Nanotechnology* 2nd edn (Berlin: Springer)
[7] Cappella B and Dietler G 1999 *Surf. Sci. Rep.* **34** 1
[8] Butt H-J, Cappella B and Kappl M 2005 *Surf. Sci. Rep.* **59** 1
[9] Garcia R and Perez P 2002 *Surf. Sci. Rep.* **47** 197
[10] Bhushan B, Israelachvili J N and Landman U 1995 *Nature* **374** 607
[11] Persson B N J 2000 *Sliding Friction: Physical Principles and Applications* 2nd edn (Berlin: Springer)
[12] Becker T and Mugele F 2003 *Phys. Rev. Lett.* **91** 166104
[13] Israelachvili J and Wennerström H 1996 *Nature* **379** 219
[14] Horn R G and Israelachvili J 1981 *J. Chem. Phys.* **75** 1400
[15] Gee M L, McGuiggan P M and Israelachvili J N 1990 *J. Chem. Phys.* **93** 1895
[16] Granick S 1991 *Science* **253** 1374
[17] Israelachvili J 1992 *Intermolecular and Surfaces Forces* (New York: Academic)
[18] Klein J and Kumacheva E 1998 *J. Chem. Phys.* **108** 6996
[19] Kumacheva E and Klein J 1998 *J. Chem. Phys.* **108** 7010
[20] Kumacheva E and Klein J 1995 *Science* **269** 816
[21] Demirel A L and Granick S 1996 *Phys. Rev. Lett.* **77** 2261
[22] Gao J, Luedtkem W D and Landman U 1997 *Phys. Rev. Lett.* **79** 705
[23] Heuberger M, Zäch M and Spencer N D 2001 *Science* **292** 905
[24] Lauga E, Brenner M P and Stone H A 2005 *Handbook of Experimental Fluid Dynamics* (New York: Springer)
[25] Neto C, Evans D R, Bonaccurso E, Butt H-J and Carig V S J 2005 *Rep. Prog. Phys.* **68** 2859
[26] de Gennes P G 2002 *Langmuir* **18** 3413
[27] Lauga E and Brenner M P 2004 *Phys. Rev.* E **70** 026311
[28] Bonaccurso E, Kappl M and Butt H-J 2007 *Curr. Opin. Colloid Interface. Sci.* **13** 107
[29] O'Shea S J and Welland W E 1992 *Appl. Phys. Lett.* **60** 2356
[30] Frank V and Butt H-J 2002 *J. Phys. Chem.* B **106** 1703
[31] Atkin R and Warr G G 2007 *J. Phys. Chem.* C **111** 5162
[32] Gosvami N N, Sinha S K, Holtbauer W and O'Shea S J 2007 *J. Chem. Phys.* **126** 214708
[33] O'Shea S J, Welland W E and Pethica J B 1994 *Chem. Phys. Lett.* **223** 336
[34] Han W and Lindsay S M 1998 *Appl. Phys. Lett.* **72** 1656
[35] Lim R, Li S F Y and O'Shea S J 2002 *Langmuir* **18** 6116
[36] Lim R and O'Shea S J 2002 *Phys. Rev. Lett.* **88** 246101
[37] Lim R Y H and O'Shea S J 2004 *Langmuir* **20** 4916
[38] Jeffery S, Hoffmann P, Pethica J, Ramanujan C, Özer H and Oral A 2004 *Phys. Rev.* B **70** 054114
[39] Antognozzi M, Humphris A D L and Milles M J 2001 *Appl. Phys. Lett.* **78** 300
[40] Li T D, Gao J, Szoszkiewicz R, Landman U and Riedo E 2007 *Phys. Rev.* B **75** 115415
[41] Maali A, Cohen-Bouchiacina T, Couturier G and Aime J P 2006 *Phys. Rev. Lett.* **96** 086105
[42] Maali A, Hurth C, Cohen-Bouhacina T, Couturier G and Aimé J P 2006 *Appl. Phys. Lett.* **88** 163504
[43] Uchihashi T, Higgins M J, Yasuda S, Jarvis S, Akita S, Nakayama Y and Sader J E 2004 *Appl. Phys. Lett.* **85** 3575
[44] Sader J E and Jarvis S P 2004 *Appl. Phys. Lett.* **84** 1801
[45] Uschihashi T, Higgins M, Nakayama Y, Sader J E and Jarvis S P 2005 *Nanotechnology* **16** S49
[46] Higgins M J, Polcik M, Fukuma T, Sader J E, Nakayama Y and Jarvis S P 2006 *Biophys. J.* **91** 2532
[47] Zhu Y and Granick S 2001 *Phys. Rev. Lett.* **87** 096105
[48] Zhu Y and Granick S 2002 *Phys. Rev. Lett.* **88** 106102
[49] Tretheway D C and Meinhart C D 2002 *Phys. Fluids* **14** L9
[50] Léger L 2003 *J. Phys.: Condens. Matter* **15** S19
[51] Ellis J S and Hayward G L 2003 *J. Appl. Phys.* **94** 7856
[52] Granick S, Zhu Y and Lee H 2003 *Nat. Mater.* **2** 221
[53] Schmatko T, Hervet H and Leger L 2005 *Phys. Rev. Lett.* **94** 244501
[54] Joly L, Ybert C and Bocquet L 2006 *Phys. Rev. Lett.* **96** 046101
[55] Joseph P and Tabeling P 2005 *Phys. Rev.* E **71** 035303R
[56] Cottin-Bizonne C, Cross B, Steinberger A and Charlaix E 2005 *Phys. Rev. Lett.* **94** 056102
[57] Craig V S J, Neto C and Williams D R M 2001 *Phys. Rev. Lett.* **87** 054504
[58] Bonaccurso E, Kappl M and Butt H-J 2002 *Phys. Rev. Lett.* **88** 076103
[59] Sun G, Bonaccurso E, Franz V and Butt H-J 2002 *J. Chem. Phys.* **117** 10311
[60] Bonacoccurso E, Butt H-J and Carig V S J 2003 *Phys. Rev. Lett.* **90** 144501
[61] Maali A, Cohen-Bouhacina T and Kellay H 2008 *Appl. Phys. Lett.* **92** 053101
[62] Lasne D, Maali A, Amarouchene Y, Cognet L, Lounis B and Kellay H 2008 *Phys. Rev. Lett.* **100** 214502

[63] Henry C L, Neto C, Evans D R, Biggs S and Craig V S J 2004 *Physica* A **339** 60
[64] Batchelor G K 1970 *An Introduction to Fluid Dynamics* (Cambridge: Cambridge University Press)
[65] Landau L and Lifshitz F 1971 *Fluid Mechanics, Theoretical Physics* vol 6 (Moscow: Mir)
[66] Horn R G, Vinogradova O I, Mackay M E and Phan-Thien N 2000 *J. Chem. Phys.* **112** 6424
[67] Brenner H 1961 *Chem. Eng. Sci.* **16** 242
[68] Vinogradova O I 1995 *Langmuir* **11** 2213
[69] Honig C D F and Ducker W A 2007 *Phys. Rev. Lett.* **98** 028305
[70] Jai C, Cohen-Bouhacina T and Maali A 2007 *Appl. Phys. Lett.* **90** 113512
[71] Israelachvili J N 1985 *J. Colloid Interface Sci.* **110** 263
[72] Tretheway D C and Meinhart C D 2004 *Phys. Fluids* **16** 1509
[73] Tyrell J W G and Attard P 2001 *Phys. Rev. Lett.* **87** 176104
[74] Agrawal A, Park J, Ryu D Y, Hammond P T, Russell T P and McKinley G H 2005 *Nano Lett.* **5** 1751
[75] Craig V S J 2004 *Curr. Opin. Colloid Interface Sci.* **9** 178
[76] Yang J W, Duan J M, Fornasiero D and Ralston J 2003 *J. Phys. Chem.* B **107** 6139
[77] Zhang X H, Maeda N and Craig V S J 2006 *Langmuir* **22** 5025
[78] Simonsen A C, Hansen P L and Klosgen B 2004 *J. Colloid Interface Sci.* **273** 291–9
[79] Zhang X H, Zhang X D, Lou S T, Zhang Y, Li M, Sun J, Li X and Hu J 2004 *Langmuir* **20** 3813